Fire Safety Journal 125 (2021) 103428

Contents lists available at ScienceDirect

Fire Safety Journal

journal homepage: www.elsevier.com/locate/firesaf

Lip-height effect in diffusive pool fires

Einar Arthur Kolstad [a,*], Vidar Frette [a], Ulrich Krause [b], Bjarne C. Hagen [a]

[a] Western Norway University of Applied Science, Campus Haugesund, Norway
[b] Otto Von Guericke University Magdeburg, Germany

ARTICLE INFO

Keywords:
Batch pool fire
Non-premixed flame
Lip height
Mass-loss rate
Heat transfer

ABSTRACT

A freeboard, lip height, from the container rim to the fuel surface affects the mass-loss rate of a pool fire. Experiments where heptane was burned in circular containers with diameter 10, 20 and 30 cm have been conducted. The results showed a decrease of up to 36% in the mass-loss rate for lip heights larger than zero. The mass-loss rate per unit area is affected by the lip height enough for it to surpass the effect of the diameter: a large-diameter pool fire with a high lip height may have lower mass-loss rate per unit area than a pool fire with smaller diameter and lower lip height. An analysis of the energy distribution for one experiment, showed that 35% of the received energy was lost to the surroundings; 30% was stored, and 35% was spent on evaporating fuel.

1. Introduction

In fire-safety calculations [1] and simulations [2], pool fires are often assumed to be well-defined fire sources with given constant heat-release rates [2]. Moreover, for many fire-related accidents, the assumption of constant heat-release rate is not correct. The fuel is, in many cases, confined and as a batch prior to ignition, and the fire will be affected by both area and boundaries as it develops [3,4]. The heat-release rate ($\dot{Q}$) is, according to Babrauskas and Peacock [5], the most important variable of a fire, governing flame temperature, flame height and smoke production. $\dot{Q}$ is in turn governed by the mass-loss rate ($\dot{m}$). If the mass-loss rate of a fire is incorrect, its dependent quantities will also be incorrect.

Several studies of pool fires report a clear difference in the behaviour of pool fires with and without a lip height, the distance from the container rim to the fuel surface. This dependency is additional to the fundamental importance of the fuel area. Blinov and Khudiakov gave a relation between pool diameter and heat-release rate for hydrocarbons [6,7]. Burgess and Zabetakis [8] examined hydrocarbons and alcohols, confirming the findings of Blinov and Khudiakov. The importance of lip height has been reported for various liquid fuels, the main trend being a decreasing mass-loss rate for increasing lip height. Artemenko and Blinov [9] used aviation fuel and isoamyl alcohol; Emmons [10] studied methanol and acetone; Liu [11] investigated ethanol and heptane; Tao et al. [12] used alcohol to examine the lip-height effect for small-diameter pool fires (diameter from 5 cm to 8 cm) and lip heights from 0.5 cm to 3 cm, and Dlugogorski and Wilson studied ethanol burning in glass, copper and mild-steel containers with a small diameter (d = 4.5 cm) [13]. Kolstad [14] reported on heptane. All reported decreasing mass-loss rate for increasing lip heights. Orloff [15] examined solid PMMA and found an increasing mass-loss rate with increasing lip height. In addition, the effect of lip height on flame shape and flame characteristics has been reported by Orloff and de Ris [16], Hu et al. [17], Liu et al. [11] and Bouhafid et al. [18]. Hayasaka [19] highlighted the importance of radiation and showed that the net heat flux is evenly distributed across the fuel surface. Akita and Yumoto [20] demonstrated the importance of convection in small methanol pool fires. Nakakuki [21–23] studied heat transfer in steady-state pool fires, while Hamins et al. [24] considered heat transfer in batch pool fires. The radiative energy flow has been studied by among others Hu et al. [25] and Shinotake et al. [26]. Joulain gave a review of pool fires studies in 1998 [27], while Hu gave a review of pool fires in 2017 [28]. Ditch et al. [29] studied highly controlled pool fires in a quiescent environment and collected data from earlier studies for comparison. There are only few studies on lip-height effects during batch pool fires.

Fig. 1 shows schematically Hottel's [30] representation of the data from Blinov and Khudiakov [6]. The regression rate of the fuel is given as a function of pool diameter. Three regions were established as indicated in Fig. 1, corresponding to laminar, intermediate, and turbulent flame. The laminar region applies for fires with pool diameter less than 0.03 m and is characterized by decreasing regression rate with increasing pool diameter. In the turbulent region, where the pool

* Corresponding author. Bjørnsonsgate 45, 5528 Haugesund, Norway.
E-mail addresses: einar.kolstad@hvl.no, eak@hvl.no (E.A. Kolstad).

https://doi.org/10.1016/j.firesaf.2021.103428
Received 11 March 2021; Received in revised form 28 July 2021; Accepted 8 August 2021
Available online 11 August 2021

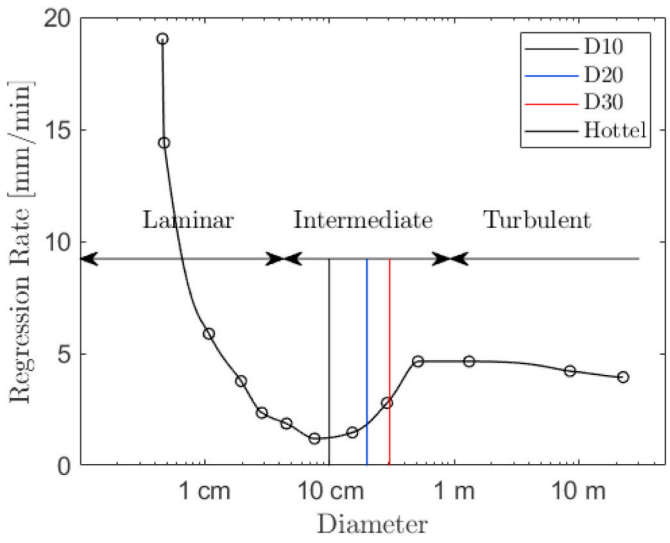

Fig. 1. Regression rate as function of pool diameter, as given by Hottel [30] (line) based on data from Bilnov and Khudiakov [7] (circles). The vertical lines indicates the container sizes explored in this article.

diameter is larger than 1 m, the regression rate becomes independent of the pool diameter. For the intermediate region, corresponding to pool diameters from 0.03 m to 1 m, the regression rate increases with increasing container diameter [m].

The experimental studies discussed above indicate that governing quantities for pool fires depend both on container size and lip height. Based on work by Zabetakis and Burgess [8] and Blinov and Khudiakov [6], Babrauskas introduced the formula in Eq. (1) for the mass flux ($\dot{m}''$), or mass-loss rate per unit area, for a pool fire as function of size [31].

$$\dot{m}''_{\text{calc.}} = \dot{m}''_{\infty}\left(1 - e^{-k\beta D}\right) \tag{1}$$

Here, $\dot{m}''_{\text{calc.}}\left[\text{kg}/\text{m}^2\text{s}\right]$ is the calculated mass flux, $m''_{\infty}\left[\text{kg}/\text{m}^2\text{s}\right]$ is the asymptotic mass flux as the container diameter increases towards infinity, k is the absorption-extinction coefficient of the fuel, β is the mean beam-length corrector [31], $k\beta$ gives the opacity of the flame [31], and D is the equivalent pool diameter.

According to Artemenko and Blinov [9], Blinov and Khudiakov [7] had initial lip heights in their experiments, without reporting them. Babrauskas acknowledged the lip-height effect for the mass-loss rate but did not take it into account. He stated that Eq. (1) is valid for pool fires with larger diameter than 20 cm, with no lip height, and unaffected by crosswind [31]. Kuang et al. [32] studied the effect of crosswind on pool fires with lip heights, showing that the mass-loss rate was highly dependent on cross air flow. In some cases, the mass flux doubled as the air flow increased from 0 m/s to 0.5 m/s.

The topic of the current work is the influence of a lip height on the mass-loss rate during batch pool fires. Systematic experiments were carried out in the intermediated regime, with pool diameters 10, 20 and 30 cm, see Fig. 1. An approximate heat balance, incorporating effects of the lip height, will also be presented.

This article is organized as follows. Section 2 describes the experimental setup and procedure. Section 3 presents the experimental results, which are further discussed in section 4. A conclusion is given in Section 5.

2. Experimental setup and procedure

The purpose of the current experiments is to investigate how lip height affects burning rates of liquids fuels. Since heptane is often used as fuel in experiments, it was also used here, being a typical liquid hydrocarbon.

The experiments were conducted by burning a predetermined amount of heptane (a batch) at a chosen initial lip height. Three circular stainless-steel containers with diameter 10, 20 and 30 cm were used, referred to as D10, D20 and D30, respectively. Three different initial configurations were investigated: heptane on top of a water layer with no initial lip height, heptane on top of a water layer with an initial lip height, and only heptane with no initial lip height. The three configurations are shown in Fig. 2. During the fire heptane was consumed, leading to an increased lip height during experiments. The batch configuration was chosen since it reflects accident scenarios and is a much-used component during fire experiments (see Section 1).

The experiments with containers initially partly filled with heptane on top of a water layer, shown in Fig. 2a and b, will be referred to as Partly Filled (PF). All PF configurations were repeated five times. The experiments with initial conditions shown in Fig. 2c will be called Burn Through (BT), since the heptane surface moved from top to bottom of the container. Each BT configuration was repeated three times.

The PF setup is shown in Fig. 3. Between the scale and the container there was an insulation block, made of a low-density fire-resistant material. Thermocouples at the rim, 4 cm from the rim at the outer wall of the container, as well as one located below the container, are shown. The thermocouples were shielded type-k elements, with outer diameter 1 mm. The scale had capacity 30 kg and resolution 0.1 g. Temperatures and mass were recorded every 5 s.

Specifications of steel containers and initial experimental conditions are given in Table 1. The lip heights are initial values. The container diameter and height are internal dimensions, and the container mass is the mass of an empty container. The heptane layer was 1 cm thick for D10 and 2 cm for D20 and D30.

A total of 134 experiments have been carried out with different container sizes and lip heights. The amount of heptane (see Table 1) in the PF experiments was chosen to obtain a burning time of around 10 min. The use of a water layer is customary for small pool fires, when they are used as well-defined fire loads in fire experiments.

All experiments were conducted under a ventilation hood, with curtains on two sides and a wall on the third side; the last side was open for observation purposes. The container was filled with the required amount of water and placed on the scale. Thermocouples were placed in position, and the scale was reset. Heptane was added to the container and recording of mass and temperatures was started 10–30 s prior to the ignition of the heptane. The heptane was ignited at the rim, with an open flame (lighter). The experiment was terminated when all fuel was consumed.

3. Results

3.1. Representative experiment

During the experiments on partly filled containers with a predetermined lip height (see Fig. 2b), four phases were observed. First, the ignition phase where the flame spread across the fuel surface within 1–2 s and the flame was located 2–5 mm above the surface. Second, the growth phase where the mass flux increased, and the flame base moved upwards and heated the container walls as it passed them. After approximately 1.5 min, the flame base was located 3–5 mm above the container rim, see Fig. 4a. The third phase is the semi-steady phase, where the mass flux was approximately constant. The flame pulsated throughout this phase (see Fig. 4), as previously reported by Orloff at el [16]. Due to the increasing lip height, the distance between the flame and the fuel surface increased during the experiment. The fourth phase is the decay phase, or burnout, characterized by rapidly decreasing mass flux. When there was only a thin layer of fuel (a few mm) left in the container, the flame base moved downwards into the container, again efficiently heating the container walls, resettling 1–2 mm above the fuel surface, and with increasing pulsation. The fuel surface started to break

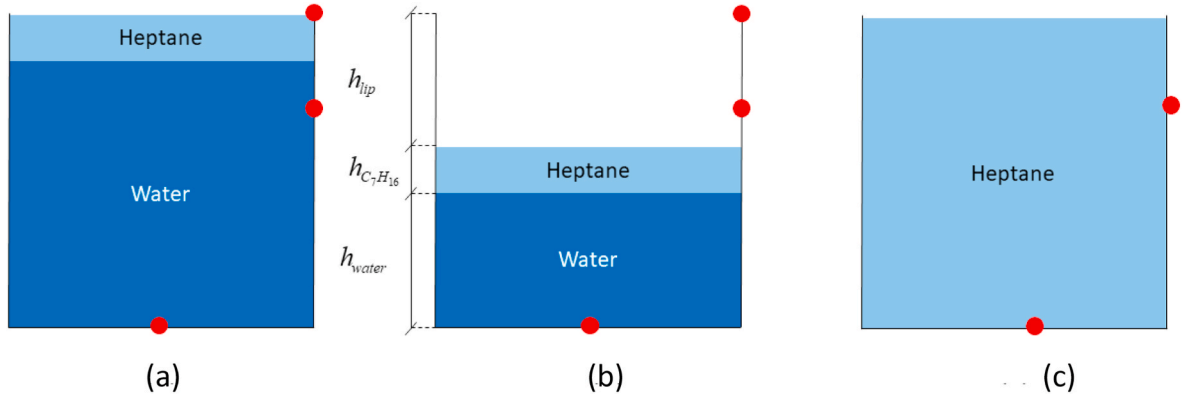

Fig. 2. Three experimental configurations were used for the current experiments: a) Zero lip height, with specified amounts of heptane and water. b) Predefined lip height with specified amounts of water and heptane. The lip height (h_{lip}) as well as the initial height of the heptane layer ($h_{C_7H_{16}}$) and the height of the water layer (h_{water}) are indicated. c) The entire container filled with heptane. Thermocouple positions are shown by red dots. (For interpretation of the references to colour in this figure legend, the reader is referred to the Web version of this article.)

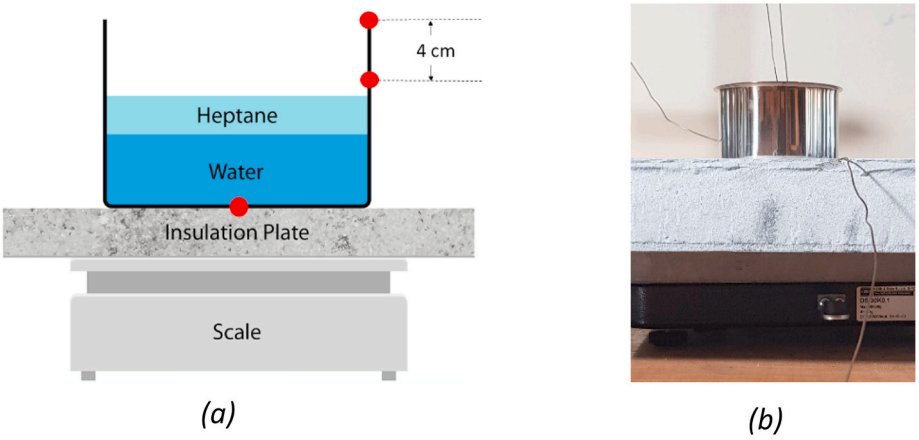

Fig. 3. (a) Experimental set-up, the red dots indicate the location of thermoelements. (b) Photograph of the setup with a 10 cm-diameter container. (For interpretation of the references to colour in this figure legend, the reader is referred to the Web version of this article.)

Table 1
Details of container and initial conditions for the experiments. In experiments as shown in Fig. 2a and b, Partly Filled (PF) experiments, a water layer was used, while experiments in Fig. 2c, Burn Through (BT) experiments, were carried out without a water layer.

Label	Container			Exp. PF Fig. 2a and b		Exp. BT Fig. 2c
	Diameter [cm]	Height [cm]	Mass [g]	Average Fuel Mass [g]	Initial Lip Heights [cm]	Average Fuel Mass [g]
D10	10	7	206	54	0, 1, 2, 3, 4, 5	389
D20	20	11.5	968	430	0, 1, 2, 3, 4, 5, 6, 7, 8	2486
D30	30	22	1839	967	0, 2, 4, 6, 8, 10, 12, 14, 16, 18	10880

up and patches of water were exposed. Eventually, all fuel was consumed and the fire extinguished. Occasionally there was draft in the laboratory during the experiments, see Fig. 4b and c. The tilt of the flame in this work is less than for flames with imposed cross air flow of 0.5 m/s as reported by Kuang et al. [32]. Pool fires affected by air cross flow of 0.5 m/s were found to have up to 100% increase in the mass flux compared with quiescent conditions. The pool fires in the current work were exposed to much weaker cross flows (drafts, see Fig. 4c) over short periods. It is therefore assumed that the small draft in the lab had little effect on the results.

The experiments with configurations shown in Fig. 2a and c had similar behaviour to those shown in Fig. 2b, PF, with the exception of the flame location during the growth phase. After ignition of a container filled to the brim (no initial lip height), the flame was located 1–2 mm above the fuel surface and the rim. During the growth phase and the semi-steady phase, the flame was located 3–5 mm above the rim as for the PF experiments. The burnout phase had similar behaviour in all three cases. Thus for Fig. 2a and c-experiments, the flame base stayed above the rim during the three initial phases, and there was no displacement of the flame base along the container as in the experiments

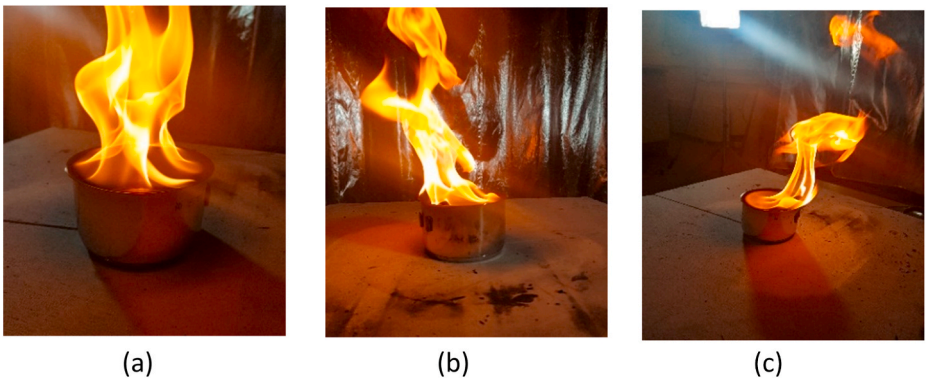

Fig. 4. D10 experiments. (a) not affected by draft and flame above the container rim. (b) affected by draft, flame partly inside the container. (c) affected by stronger draft than in part b, flame above the rim.

shown in Fig. 2b.

After completing the PF experiments shown in Fig. 2a and b, the water temperature was measured 1–2 mm below the water surface showing typically values of 75 ± 5 °C. At 1 cm below the water surfaces the temperature was 35 ± 5 °C. After these measurements, the water was stirred to obtain a homogenous temperature distribution, with typically temperature of 35 °C. The temperature measured below the container changed little (up to 5 °C increase) for experiments with water layer thicker than 2 cm. With less water (higher initial lip height, see Fig. 2b) the temperature at the bottom could increase by 20 °C during burning.

Typical behaviour of mass as function of time is shown in Fig. 5a. This is a D10 experiment with initial lip height (ILH) zero, 6 cm of water and 1 cm of heptane. The graph in Fig. 5a is slightly curved, which indicates that the mass-loss rate was not constant during this batch pool fire. The 240 s wide averaging window showed in Fig. 5a is the time span used to calculate the average mass flux for a single experiment ($\dot{m}''_{\text{avg, singel}}$). Several methods for obtaining an average mass flux have been considered, but there are only small variations in the results.

The difference in mass between two successive measurement points was divided by the time between the points, and further divided by the container area. This gave the mass-loss rate per unit area or mass flux ($\dot{m}''$), which is shown in Fig. 5b as black dots. There were large variations in the mass flux between two time-steps. A fifth-order polynomial fit was introduced to represent the mass flux (red curve in Fig. 5b). The three main phases during a pool fire can be distinguished in Fig. 5b, namely growth, semi-steady-burning, and decay phase. During the growth phase, in this case the first 125 s, the mass flux increased. The growth phase was followed by the semi-steady-burning phase, lasting until 480 s. During this phase, the mass flux decreased from 16.4 g/m^2s to 9.7 g/m^2s, which is a reduction of 41%. During the decay phase, lasting from 480 s to burnout at 560 s, the mass flux decreased rapidly towards zero. This phase is characterized by reduced evaporation of fuel and a weaker flame.

3.2. Mass-loss rate

As explained in the introduction, the heat release rate is the most important variable in fire safety, and the heat-release rate can be calculated from the mass-loss rate.

3.2.1. Partly Filled experiment

Fig. 6 shows a selection of experiments with given diameter and initial lip height. The chosen experiments are for zero initial lip height (the lowest possible), 2 cm (the second lowest initial lip height tested for all three diameters), and finally an initial lip height corresponding to 40% of the diameter (the highest value tested for all diameters). The direct (unsmoothed) mass flux (black dots) in Fig. 6, was calculated as described in Section 3.1 (see Fig. 5b), for the given values of initial lip height and diameter. The red line is a fifth-order polynomial fitting of

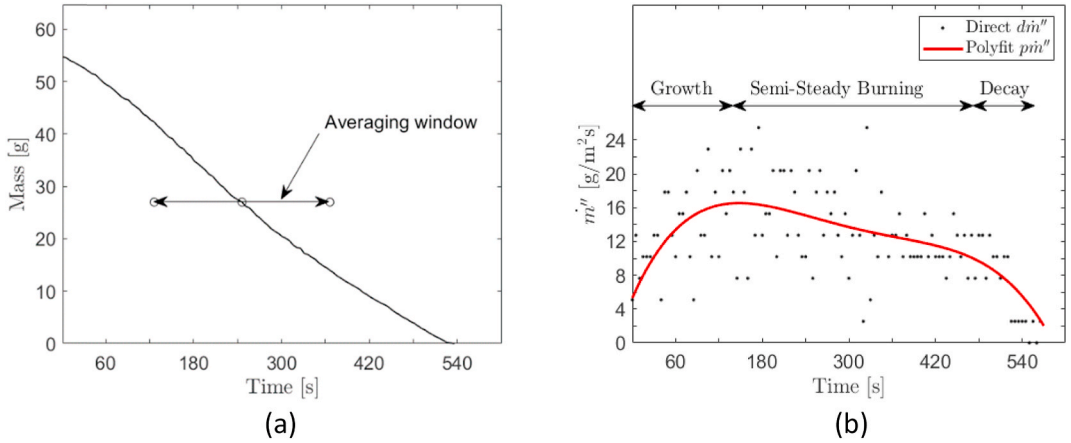

Fig. 5. A D10 experiment with heptane and water layers, but without initial lip height, as shown in Fig. 2a. Part (a): Mass as function of time. The Aaveraging window was used to calculate an average mass-loss rate. The averaging window extended from 2 min before to 2 min after the time where half the heptane mass had been consumed. Part (b): Direct $\dot{m}''$ calculated from the recorded mass data using every value (black dots). The main phases that a fire undergoes are marked with "growth", "semi-steady burning" and "decay", as discussed in the main text. The red curve is explained in the main text. (For interpretation of the references to colour in this figure legend, the reader is referred to the Web version of this article.)

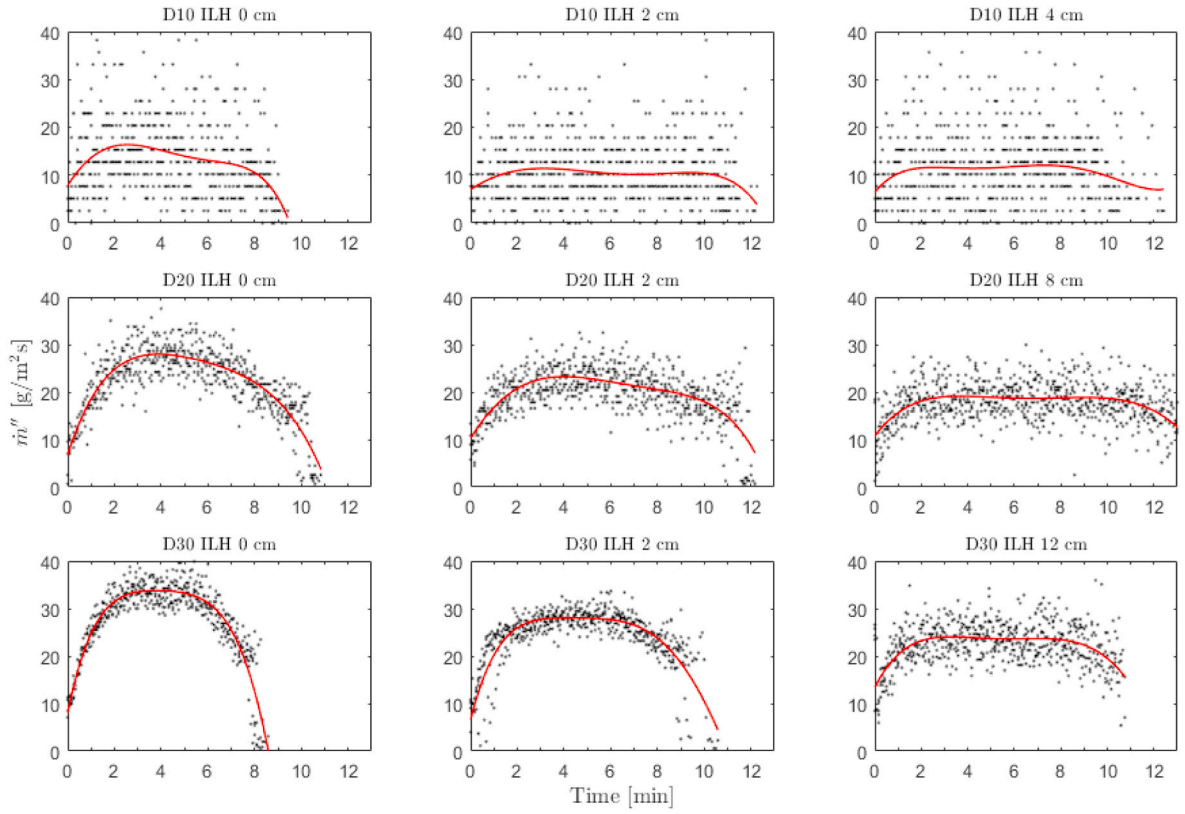

Fig. 6. Direct calculated mass flux with its fifth-order polynomial fitting for given diameter (D) and initial lip height (ILH).

the data represented by the black dots, which are all measurement points for all experiments with the same diameter and initial lip height. In Fig. 6, the zero ILH configuration has a shorter and less obvious steady burning region for all container diameters. With higher ILH, the semi-steady phase lasted longer and is easier to distinguish, in particular for ILH at 40% of the diameter (third column in Fig. 6) and higher (data not shown), for all three diameters.

Experiments were carried out with five runs for each pool size and initial lip height. Using the averaging window from Fig. 5a, an average mass flux for each experiment was calculated, and the results are shown in Fig. 7, with mass flux as function of average lip height. The average lip height was calculated as the average of initial and final lip height. Fig. 7 shows $\dot{m}''_{\text{avg, singel}}$ for all experiments carried out in this study. For all three container sizes (D10, D20 and D30), the mass flux decreases with increasing lip height, but for D10 there is an increase again when the initial lip height exceeds 4 cm. A similar but weaker increase for the highest values of the lip height can be distinguished for D20, possibly also for D30. Factors that may explain such a behaviour are discussed in Section 4.1. The spread in mass flux between the five experiments with identical conditions increases with increasing lip height for all container sizes. The largest spread occurs for D30 containers, where the mass flux varied between 33 and 36 g/m^2s for initial lip height 0 cm, and between 18 and 28 g/m^2s for initial lip height 16 cm.

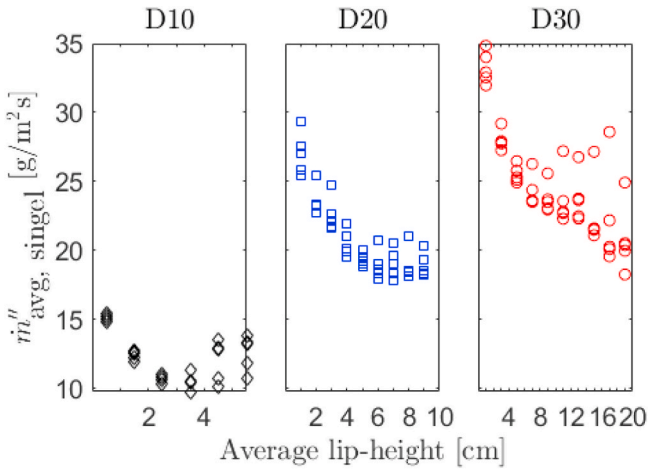

Fig. 7. The mass flux for all experiments as function of average lip height during the run for all experiments. The mass flux was calculated using the averaging window discussed in the main text.

Fig. 8a shows $\dot{m}''_{avg}$, which is $\dot{m}''_{avg,\ singel}$ averaged over the five experiments with identical initial conditions, and the corresponding standard deviation. Lip heights in Fig. 8 are average lip heights, e.g., for 2 cm initial lip height, and 1 cm heptane layer, the average lip height was 2.5 cm. The three data sets show a similar reduction in $\dot{m}''_{avg}$ (with approximately the same slope) up to lip height 3 cm.

In Fig. 8a, $\dot{m}''_{avg}$ of D10-fires seems dependent on lip height for the full range investigated. For D20-fires the mass flux becomes independent of lip height for values greater than 5 cm. D30-fires are independent of the lip height between 5 and 13 cm. Based on these experiments, there is no unique lip height where the mass flux becomes independent of the lip height. Whether there is a finite lip height, where the fire extinguishes needs to be investigated. Work by Liu et al. indicates that such a limit exists for steady-state pool fires [11].

In Fig. 8b the dimensionless mass flux was obtained by dividing the mass flux from Fig. 8a by the mass flux of the experiment with initial lip height 0 cm. The dimensionless lip height is the lip height divided by the container diameter. Fig. 8b shows a reasonable data collapse for all container diameter and lip heights, with exception of D10 with dimensionless lip height above 0.4.

3.2.2. Burn through experiments

The Burn Through (BT) experiments (heptane only, no initial lip height and no water layer) lasted until all fuel was consumed. In Fig. 9a, recorded mass is shown as a function of time for three experiments, denoted D10_BT, D20_BT and D30_BT, with container diameters 10, 20 and 30 cm, respectively. Note the significant difference in mass-loss rate (negative slope) between the three container diameters. D30_BT has a (negative) slope 14 times larger than D10_BT.

The Burn through (BT) experiments had a large variation in lip heights, from 0 cm to 7, 11.5, and 22 cm for D10, D20, and D30, respectively (see Table 1). Therefore, mass flux and lip height from these experiments are given as time-varying quantities. The mass flux for BT experiments was calculated in three steps. First, $\dot{m}$ for a single experiment was calculated for each time step, these data were fitted using a fifth-order polynomial, and $\dot{m}''$ was calculated as a function of time from brimful to empty container. Finally, the mass flux averaged over the three experiments with identical starting conditions, was calculated for each lip height, together with the standard deviation, see Fig. 9b.

The increase in $\dot{m}''$ early in the experiments, see Fig. 9b, was due to fire growth. During the growth phase, the flame heated the liquid surface leading to increased evaporation of fuel. The growth phase ended when the fuel surface temperature reached the boiling point. After the growth phase, there was a period with decreasing $\dot{m}''$. From the point where the lip height was approximately half the container height, $\dot{m}''$ continued to decrease, but at a lower rate. Just before burnout, $\dot{m}''$ increased slightly, which corresponds to the time where the flame re-entered the container.

3.3. Temperatures

Temperatures at the outer wall of the container were measured for both Partly Filled (PF) and Burn Through (BT) experiments. For the PF experiments, thermocouples were placed at the rim, 4 cm from the rim and below the container. For BT experiments, one single thermocouple was placed 4 cm from the rim. Red dots in Fig. 2 indicate the position of the thermocouples. To compare PF and BT experiments the temperature evolution for representative experiments is presented in Fig. 10 (PF) and Fig. 11 (BT).

3.3.1. Temperature during Partly Filled experiments

Fig. 10 shows how temperatures at the rim, wall, and below the container changes with time, for nine single PF-experiments with different initial lip heights. Fig. 10a shows an increase in temperature with time for all PF-experiments. After ignition, two types of temperature evolution can be distinguished. Firstly, for initial lip heights of 0, 1 and 2 cm, there was first a strong increase in temperature directly after ignition (for about 1 min) followed by still increasing temperatures, but at a lower rate. Secondly, for experiments with initial lip heights 3–8 cm, there was first a fast temperature increase of several hundred degrees during the first minute after ignition. During the next 5–6 min, temperatures decreased by 10–100 °C. The temperature increase was largest for the highest initial-lip values. From 5 to 6 min onwards, the temperature increased by 10–50 °C.

Fig. 10b shows temperatures at the container wall (4 cm) for the nine PT-experiments. Two distinct groups of curves, with initial liquid surface located above and below the measuring point at 4 cm, respectively. For initial liquid surface located above the measurement point (initial lip height 3 cm or less) there is a slow increase in the temperature. Near the end, there is a distinct increase in temperature for initial lip height higher than 2 cm, but not for 0 and 1 cm, probably because the water layer for these cases extended above the measurement point (at 4 cm). All experiments with an initial liquid surface at and below the measuring point show a rapid increase in the temperature during the first 30–40 s. In the 5–8 cm initial lip height experiments, the initial rise was followed by 2–3 min with decreasing temperature, before the temperature stabilized and then increased. The curves are systematically ordered, with

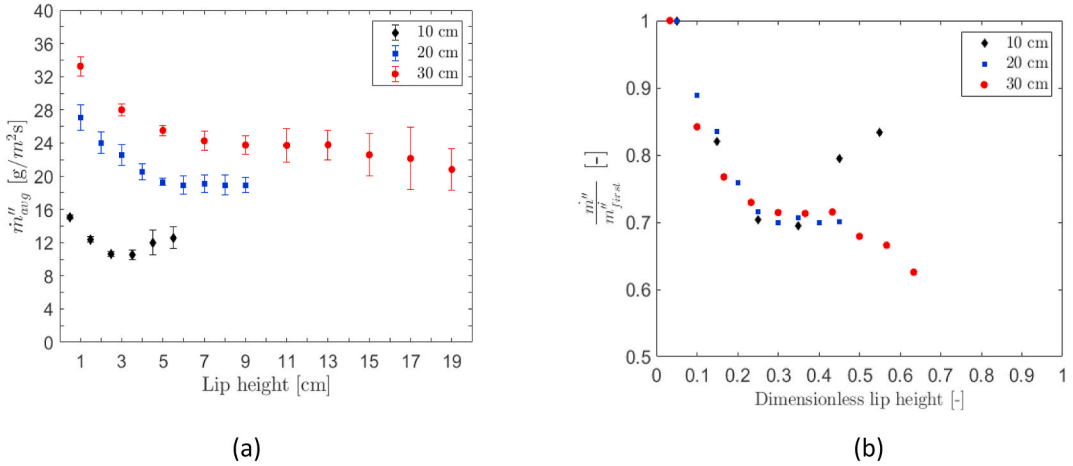

Fig. 8. Mass flux for partly filled containers with diameter 10, 20 and 30 cm (a) $\dot{m}''_{avg}$ as function of lip height. Each data point shown was obtained by averaging $\dot{m}''_{avg,\ singel}$. (b) Dimensionless mass flux (data from (a) divided by the mass flux of the experiment with initial lip height 0 cm) as function of dimensionless lip height. The dimensionless lip height is the lip height divided by the container diameter.

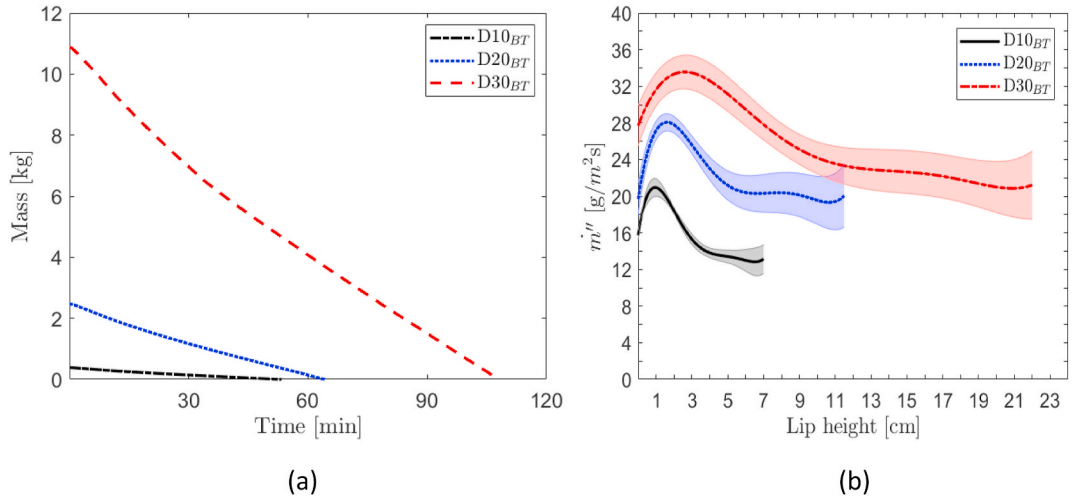

Fig. 9. (a) Mass as function of time for experiments with only heptane in the container. Each experiment was started with a completely full container and allowed to burn till all fuel was consumed (burn-through experiments). (b) fifth-order polynomial regression of $\dot{m}''$ for burn-through experiments as function of lip height. The graphs were determined by averaging data from the three repetitions for each container diameter. The shadow indicates one standard deviation at each side.

lowest temperature for the lowest initial lip height and highest for the highest lip height, probably due to the heat sink effect of the water layer. 2–3 min before burnout, when the flame front moved back into the container, there was a distinct growth in the temperature for experiments with initial lip height from 3 to 8 cm.

Comparing Fig. 10a and b, the curve shapes are similar, but the temperature values are much higher in Fig. 10a. This is reasonable since the measuring point for the curves in Fig. 10a is closer to the flame during most of the experiments. The order of the curves (in vertical direction) is also similar but not identical.

Fig. 10c shows the temperature below the container, which increased only around 5 °C throughout the experiments. The difference in initial temperatures reflects laboratory temperature. The exception from a 5 °C-bound on the temperature increase is the experiment with initial lip height 8 cm, where the temperature increased with approximately 20 °C during the experiment. This larger increase is probably due to the small amount of water used in this experiment, with less heat sink effect (D20 is 11.5 cm deep, see Table 1, giving a water layer of 1.5 cm).

3.3.2. *Temperatures during Burn Through experiments*

Fig. 11 shows how the temperature 4 cm from the rim evolved during the BT-experiments. Even with three different container sizes, the temperature development at 4 cm seems to be similar and not dependent on container size.

A relatively slow increase in temperature can be observed for lip heights less than 3 cm. However, from lip height 3 cm and onwards the temperature increased more rapidly, despite the heptane surface still being above the measurement point 4 cm below the rim. It is likely that the flame had begun heating the heptane layer 4 cm below the rim, and that the heptane acted as a heat sink, with moderate temperatures in the container walls from the heptane surface and downwards. For the D10-pan the temperature increase continued at the same rate after the lip height had passed 4 cm and down to about 7 cm. At the end of all experiments, there was a rapid increase in temperature. Two aspects of these experiments probably contributed to this rapid increase. First, during this final stage of the experiments, the flame moved from the rim of the container down towards the heptane surface. During this transition, the flame heated the container wall, in particular the region near the measurement points 4 cm below the container rim. Second, the combustion rate increased during this late stage. The remaining fuel layer was thermally thin and at or very near the boiling point. Thus, the heat supplied to the fuel layer from container walls and flame was used for evaporation, whereas during previous stages, heat was also spent on preheating fuel. Due to the relative values of specific heat and latent heat of evaporation for heptane (as reflected in the so-called Maximum-burning-rate ratio), this led to an increased combustion rate [19]. For D30 sharp oscillations in temperature occurred between 16 and 17 cm.

4. Discussion

In all, 134 experiments have been conducted. The results presented in Figs. 7–9 show that larger lip height leads to a lower mass flux. This is in agreement with findings from Lui et al. [11], Kolstad et al. [14], Orloff [15] and Bouhafid et al. [18].

Five important aspects of the results will be discussed in more details: a comparison of the current results with the mass-flux equation (Eq. (1)), temperature evolution for different lip heights, comparison of Partly-Filled (PF) and Burn -Through (BT) experiments, comparison of steady-state and batch pool fires, and the energy distribution from the flame to the container with water and heptane.

4.1. *Mass flux: experiments versus mass-flux equation*

In Fig. 12, data from Fig. 8 are plotted together with $\dot{m}''_{calc}$ for heptane from Eq. (1), with $\dot{m}''_{\infty} = 101$ g/m^2s and $k\beta = 1.1$ m^{-1} [33]. Values for D10 have also been included even though they are outside the range of the equation. Fig. 12 suggests that Eq. (1) does not represent mass flux obtained for D20 and D30 containers with no initial lip height.

In Figs. 8a and 12, the average lip height was used for each experiment. As explained in Section 3.2.1, this quantity was obtained as the average of initial and final lip height. This leads to a true average lip height if the mass flux is constant throughout each experiment. Fig. 6 shows that this is not strictly the case. However, considering the fifth-order polynomial for many experiments the mass flux was reasonably close to constant, particularly for higher values of the initial lip height. Moreover, for a symmetrical mass-flux curve, the averaging used will also lead to the true average lip height. Several mass-flux curves in Fig. 6 are also rather symmetrical. Thus, the simple scheme used to calculate the average lip height, is expected to give results close to the true values.

Artemenko and Blinov [9] stated that Blinov and Khudiakov [6,7] often used partly filled containers in their work. Thus, they did not distinguish clearly between completely-filled and partly-filled containers. It is therefore interesting to note that there is a reasonable agreement between Eq. (1) and the experimental values in Fig. 12 for lip heights 2–4 cm. In particular, this applies for the D10 experiments,

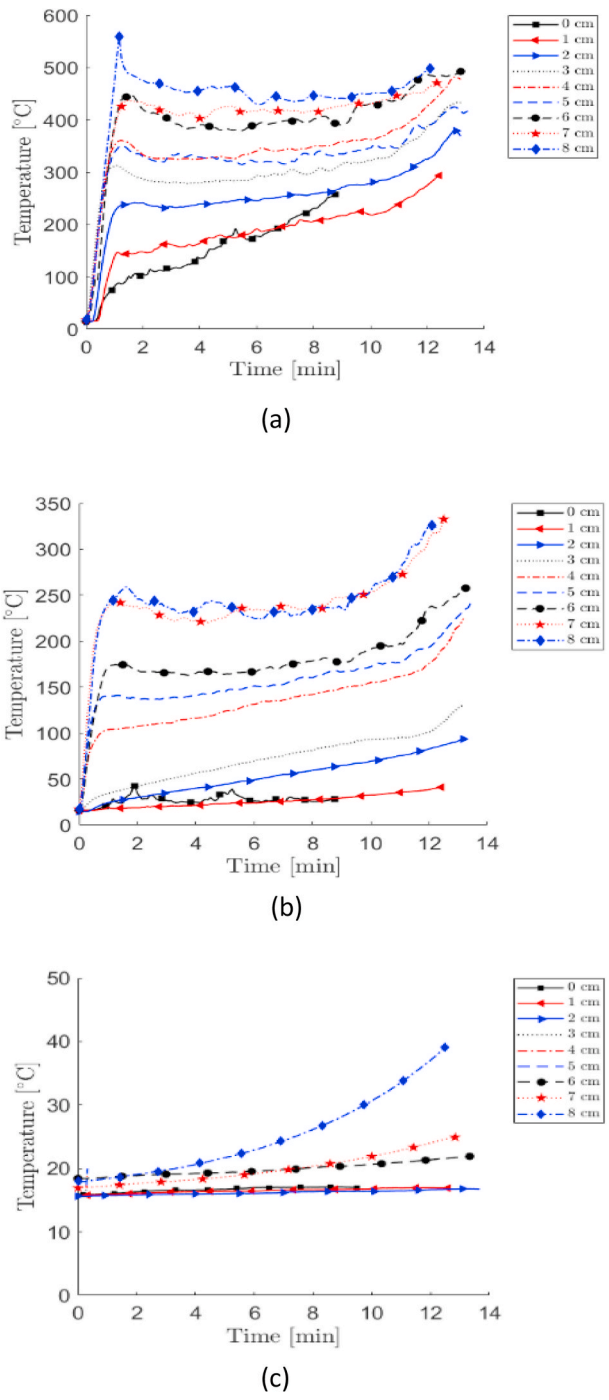

Fig. 10. Temperature measurements from nine D20 Partly Filled experiments. (a) Temperatures at the container rim. (b) Temperatures 4 cm below the container rim, at the outer container wall. (c) at the container bottom, measured beneath the container.

which are outside the range of validity (in terms of diameter) of Eq. (1).

Fig. 6 showed that PF experiments with low initial lip height did not have a distinct steady burning region. The mass flux for D10 with 0 cm initial lip height decreased by 40% during the semi-steady region, while for D20 and D30 with no initial lip height the fifth-order polynomial curve is similar (but not equal) to a parabola. It is therefore unclear whether the burning time was sufficient to obtain steady burning for the PF experiments with 0 cm initial lip height. For the BT experiments in Fig. 9b, there are large variations in the mass flux as the initial lip height increases from 0 cm to 4, 6 and 11 cm, for D10, D20 and D30, respectively. It is therefore reasonable to conclude that it would be difficult to obtain a true steady burning phase for batch pool fires with small lip heights.

In Fig. 12, the decreasing trend for the mass flux as function of lip height is followed by an increase for the highest values of the lip height. This is obvious for D10, but can also be distinguished for D20, possibly also for D30 (see Fig. 7). Two factors may explain this behaviour. Firstly, D10 is more dependent on conductive and convective heat transfer than the larger containers. Secondly, the water layer is thin for the experiments with the highest initial lip height: 1 cm, 1.5 cm, and 2 cm, for D10, D20 and D30, respectively (see Table 1). This may lead to a higher water temperature and enhanced fuel evaporation. A markedly higher

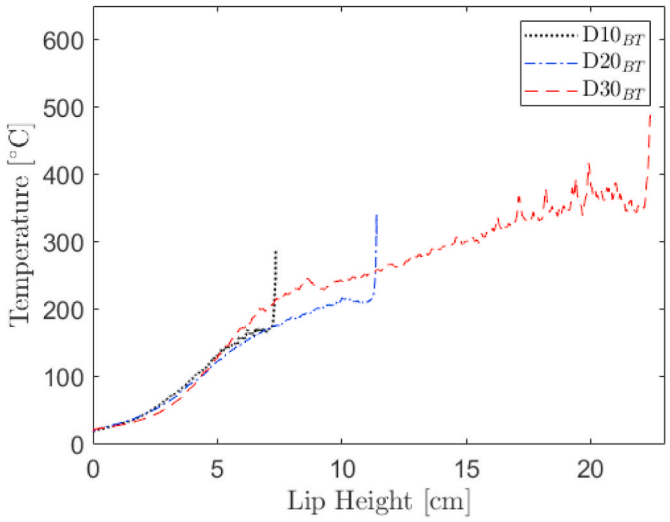

Fig. 11. Temperature 4 cm from the rim for three burn-through experiments, one of each container size.

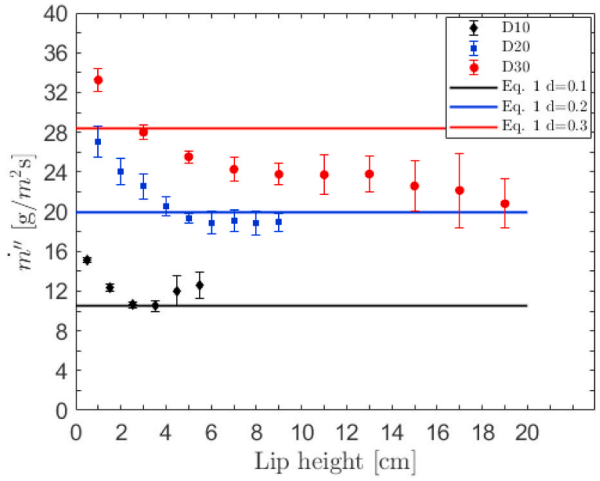

Fig. 12. *Average $\dot{m}''$ as function of lip height compared with $\dot{m}''_{calc}$ calculated from Eq., with $\dot{m}''_{\infty} = 101$ g/(m^{2}s) and $k\beta = 1.1$ m^{-1}.*

temperature was indeed found for the largest initial lip-height value (8 cm) in Fig. 10c. Furthermore, the increase in mass-loss rate is strongest for D10, with the thinnest water layer, and becomes less pronounced for D20 and D30, as the water depth increases.

4.2. Temperatures

The evolution of temperature as a function of time, as shown in Figs. 10 and 13, may be understood from the location of the flame, combined with heat absorption in the water layer and container. After ignition, the flame was located 1–2 mm above the fuel surface. During the first minute, the fuel evaporation increased. Oxygen influx is required to maintain combustion. Since the flame covered the cross-section of the container, and (for PF experiments) evaporated fuel filled the container above the liquid surface with the fire plume, there was a lack of oxygen inside the container. When the flame had consumed the available oxygen inside the container it moved up towards the container rim where more oxygen was available. As the flame front reached the container rim, the flame volume increased and obtained a cylindrical/conical shape until the flame surface area was large enough to combust all the gas flowing from the pool. From this point on, the flame remained fixed 3–5 mm above the container rim.

The temperatures in the PF experiments increased rapidly in the beginning since the flame started at the fuel surface inside the container and moved upwards to the rim, heating the wall in passing. Then the increase becames lower before a new rapid increase at the end when the flame re-entered the container and once again heated the container walls. For experiments with initial lip height lower than 2 cm there was only a moderate temperature increase (5–65 °C). Interestingly, the series of PF curves in Fig. 13 agree (when the initial near-vertical portions are neglected). However, the PF curves differ significantly from the BT-curve. The BT experiment had a lower temperature increase during most of the experiment and a rapid increase towards the end of the experiment. The water level determines the temperature evolution in the PF experiments. If the thermocouple at 4 cm was located above the liquid surface level (only gas on the opposite side of the wall), there was a rapid temperature increase in the beginning and at the end of the experiments. These temperature increases correspond to flame motion first upward and at the end downwards along the container wall. This behaviour was not present when the thermocouple was located below the water level. For BT experiments, the initial rapid temperature increase was not present since the flame did not move upwards but stayed above the container rim until the last phase of the fire. Temperature as functions of lip height is shown in Fig. 13. The lip height was estimated from mass and the density of heptane. Heptane has a thermal expansion coefficient of 0.00124 $^1/_K$, which gives an error in the estimated lip height of approximately +5–10% when the temperature reaches 100 °C.

4.3. Mass flux: Partly Filled versus Burn Through

In Fig. 14, results on the mass-loss rate per unit area (mass flux) from the PF and BT experiments are plotted together. For small lip heights (0–3 cm), the mass flux for the BT experiments was higher than for the PF experiments, while for larger lip heights (above 5 cm) the difference between BT and PF is reduced.

It could be reasonable to expect that the mass flux for BT and PF experiments as function of lip height would be similar over the entire range of lip height. That is, under the assumption that a BT experiment would experience the same condition as several PF experiments as it propagates from top to bottom of the container. However, both the results in Fig. 14 and the differences in temperature evolution discussed in Section 4.2 demonstrate that such an assumption cannot be made. Several factors lead to enhanced evaporation and higher mass-loss rate for a BT experiment compared with the corresponding PF experiments. During a BT experiment, the flame transferred heat to the container wall over a longer period than in the PF experiments, also each PF started with cold container walls. The flame motion inside the container, from the rim to the fuel surface, also differs in the two cases, as discussed above. Even with the difference in mass flux for PF and BT -experiments, the mass flux for the two types of experiments converge as the lip height increases. D20 converge from around 6 cm and D30 at 11 cm. This may reflect that an equilibrium has been reached between heat received by and emitted from the container wall.

Thus, the systematic difference between the BT and PF experiments in Fig. 14 points to the importance of understanding heat transfer and heat storage during pool fires. A simplified analysis is given in Section 4.5.

4.4. Comparison with the study by Liu et al

Liu et al. has conducted experiments on steady-state pool fires with various lip heights [11] in containers with diameter 10, 15 and 20 cm. The mass fluxes from their study of containers with diameter 10 and 20 cm is compared with the results from this work in Fig. 15. The steady-state pool-fires have lower mass flux than the batch pool fires with similar container diameter and (average) lip height. For both

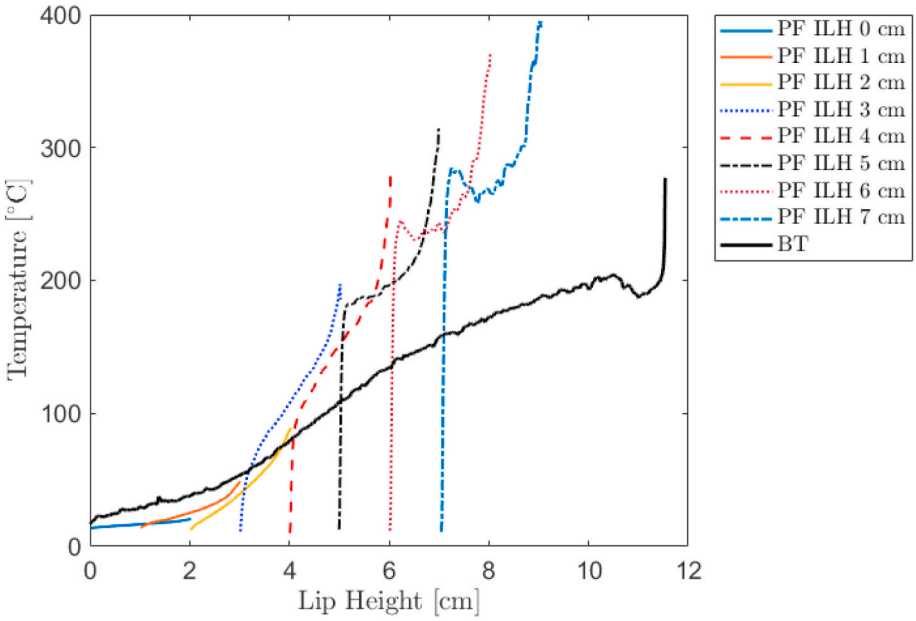

Fig. 13. Temperature 4 cm below the rim, as function of lip height for Partly Filled (PF) experiments, and a Burn-Through (BT) experiment. Both BT and PF experiments were conducted in the container with diameter 20 cm. The PF experiments had different Initial lip heights (ILH), as given in the legend.

steady-state and batch pool fires the mass flux decreases with increasing dimensionless lip height. Batch pool fires have a steep decrease in mass flux for nondimensional lip heights up to 0.25; then D20 becomes independent of lip height. D10 has a small increase in the mass flux. Steady-state pool fires have a continuously decreasing mass flux with increasing lip height.

Fig. 15b shows the percentage deviation of results reported in this article from Liu et al., with a difference from 20 to 55% between steady-state and batch pool-fires. For the smallest dimensionless lip height D10 experiments deviate 40% while D20 experiments deviate 50% from each other. The deviation decreases with increasing dimensionless lip heights up to 0.4. For D20 with dimensionless lip height at 0.4 the deviation is 40% and for D10 with dimensionless lip height at 0.45 the deviation is 55%.

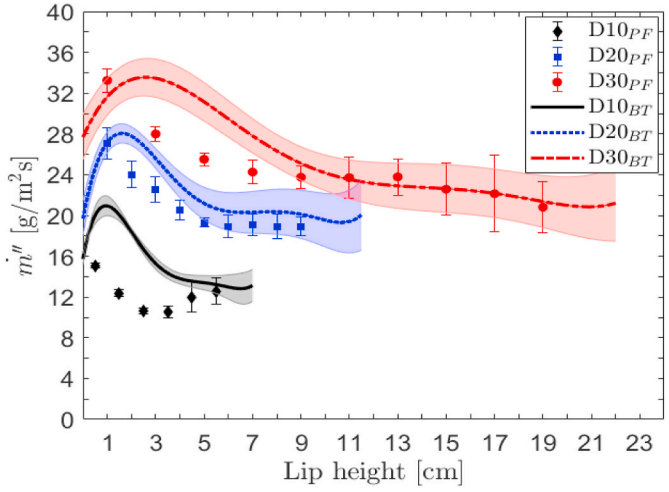

Fig. 14. Mass flux as function of lip height for all experiments. The curves are polynomial fitting to $\dot{m}''$ for Burn Through (BT) experiments, see Fig. 10. The filled circles, squares and diamonds with error bars are $\dot{m}''$ for Partly Filled (PF) experiments, see Fig. 8.

4.5. Energy balance

To get a better understanding of the different energy fluxes in batch pool fires and how energy is redistributed in the fire-heptane-container system, a simplified energy balance will be presented. More advanced models are presented by Nakakuki [21–23] (steady-state pool fires) and Hayasaka [19] (batch pool fires).

An energy balance gives an overview of the heat flows during a fire. In pool fires, energy is radiated from the flame in all directions. A fraction of this energy reaches the fuel surface (heptane) through direct radiation and indirectly by radiation to the container wall, followed by conduction through the wall and radiation from the wall (above the fuel level) to the fuel. A part of the energy that reaches the container wall is lost to the surroundings by radiation and some of it will heat the fuel and water layer (if present) through conduction. These energy flows are important for the overall energy balance of the system: fuel, water, and the container. Here, estimates of energy flows will be given based on the D20 experiment with initial lip height 5 cm. Fig. 16 shows the relevant energy flows. In addition, heating of the container, water, and fuel are important parts of the heat balance. Due to conservation of energy, thermal radiation from the fire ($\dot{Q}_F$) must be equal to the sum of energy ($\dot{Q}_U$) used to evaporate the fuel ($\dot{Q}_V$), energy lost or emitted from the system ($\dot{Q}_L$) and energy stored in the system $\left(\dot{Q}_S\right)$, see Eq. (2). In Fig. 16, F indicates thermal radiation from the flame to system $\left(\dot{Q}_F\right)$, V the energy required to evaporate heptane ($\dot{Q}_V$) at a certain rate, and L the energy flow from the system to the surroundings (heat losses), $\left(\dot{Q}_L\right)$. Heat losses occur mainly through convection and radiation, as described below. The stored (released) energy ($\dot{Q}_S$), as parts of the system are heated (or cooled down), is not indicated in Fig. 16. Heat losses occur mainly through convection and radiation, as described below.

$$\begin{aligned} \dot{Q}_F &= \dot{Q}_U \\ \dot{Q}_F &= \dot{Q}_V + \dot{Q}_S + \dot{Q}_L \end{aligned} \tag{2}$$

There are also conductive heat losses through the container bottom. Since the temperature difference between container and insulation plate is small (see Fig. 10c), this contribution will not be included.

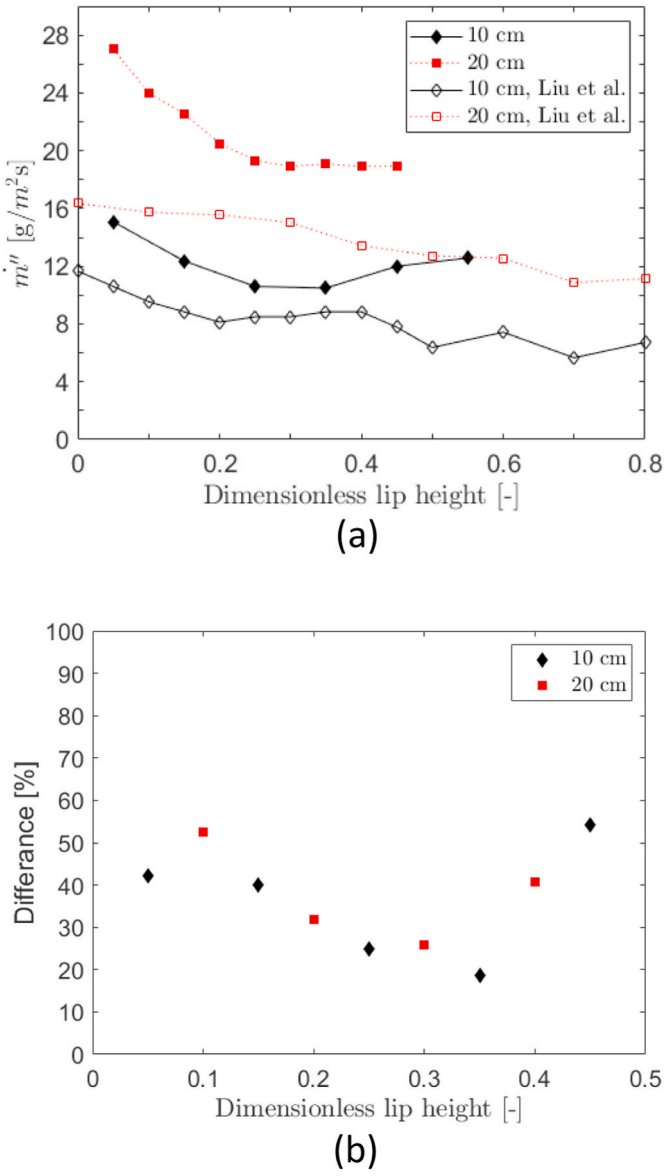

Fig. 15. (a) Dimensionless mass-loss rate as function of dimensionless lip height compared with Liu et al. [11]. This work has solid points while Liu et al. has open points. (b) per centage deviation of this work from Liu et al.

Physical values used in the calculations below are listed in Table 2. The values are collected from literature (see references in Table 2) and experimental results from this work. For values with significant uncertainty, such as the radiative fraction, a range of values is given in Table 2. The latent heat of evaporation varies from 317 to 364 $^{J}/_{kgK}$, for liquid (fuel) temperature 98 °C and 30 °C, respectively. The mass flux (17.9-20.7 $^{kg}/_{m^2s}$) extends from the lowest to the highest mass flux obtained in this work. The mass of the hot and cold parts of the container is calculated as follows. The mass of the container from the bottom to the liquid surface (cold part) and from the fuel surface to the rim (hot part) is equal to the container mass in Table 1. The same approach was used to calculate the area of the hot container wall $A_{w,1}$, while the A_w is the total area of the container wall. The burning time of 820 s is the burning time of the experiment used in this calculation.

The thermal radiation from the flame to fuel and container, can be estimated using the energy release from the fire and view factors. The total heat-release rate, $\dot{Q}$, for a fire is given by Eq. (3) [33].

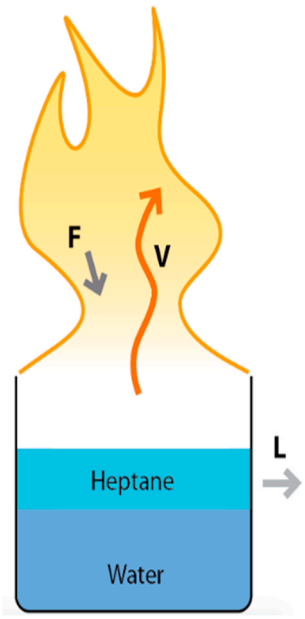

Fig. 16. Schematic presentation of relevant heat and mass fluxes, F is radiation from the flame, V is evaporation of the fuel (heptane), L is heat losses from the container to the surroundings.

$$\dot{Q} = \chi_{\text{eff}} \cdot \dot{m}'' \cdot A \cdot \Delta H_C \tag{3}$$

Here, χ_{eff} is the combustion efficiency, $\dot{m}''$ is the mass flux, A is the pool surface area, and ΔH_C is the heat of combustion. With the given values $\dot{Q}$ is then 19 ± 1.4 kW.

$\dot{Q}_f$ is the radiative part of $\dot{Q}$ as given in Eq. (4).

$$\dot{Q}_f = \chi_{\text{rad}} \cdot \dot{Q} \tag{4}$$

Using Eq. (4), $\dot{Q}_f$ is 6.3 ± 2.8 kW. The radiation reaching the system ($\dot{Q}_f$) is governed by the geometrical view factor as given in Eq. (5).

$$\dot{Q}_F = \varphi_{F\to C} \cdot \dot{Q}_f \tag{5}$$

φ with subscript F (flame) to C (container with contents) is the view factor from the flame to the system. It is assumed that the flame has a shape such that it does not radiate to the outer container wall.

To determine φ, the inner area of the flame, A_F was found using the model of Shen et al. [38] for flame shape. Shen et al. assumed that the flame can be approximated by two geometrical objects, a cylinder (the continuous flame) and a cone (the intermittent flame). The base of the cylinder and of the cone are assumed to be equal to the container diameter. The heights are shown in Fig. 17 as intermittent(h_I), and continuous (h_C) flame height, representing the heights with flames present at least 95% and 5% of the time, respectively. Fig. 18 shows the approximation proposed in Ref. [38] for the complex, continuously changing flame shape in real cases, as illustrated in Fig. 17.

Eq. (6) is the Heskestad equation for mean flame height (L) defined as the height with flames 50% of the time [39].

$$L = 0.235 \cdot \dot{Q}^{2/5} - 1.02D \tag{6}$$

Here, L is the average flame height, $\dot{Q}$ is the energy production, and D is the pool diameter. The flame height for the $D20_{PF}$ experiments becomes 0.57 m. Eq. (7) gives the relationship between L, h_I, and h_C as described by Shen et al. [38].

Table 2
Values used in calculations.

Properties	Symbol	Value	Unit	Ref
Heptane				
Combustion effectivity efficiency	χ_{eff}	0.69	–	[33]
Radiative fraction	χ_{rad}	0.2–0.45	–	[33]
Net heat of combustion	ΔH_C	44600	kJ/kg	[33]
Latent heat of evaporation	L_V	317–364	kJ/kg	[34]
Heat capacity heptane	$C_{p,h}$	224.6	$J/kg{\cdot}K$	[35]
Mass flux	$\dot{m}''$	17.9–20.7	g/m^2s	Fig. 7
Steel container				
Emissivity steel container	ε_s	0.39	–	[36]
Heat capacity steel	$C_{p,s}$	480	$J/kg{\cdot}K$	[37]
Mass container, hot part	$m_{c,h}$	0.276	kg	Table 1
Mass container, cold part	$m_{c,c}$	0.692	kg	Table 1
Water				
Heat capacity water	$C_{p,w}$	4181	$J/kg{\cdot}K$	Table 1
Mass water	m_w	1.26	kg	Table 1
Other				
Container cross-section area	A	0.031	m^2	Table 1
Area of outer container wall	A_w	0.072	m^2	Table 1
Area of hot container wall	$A_{w,1}$	0.035	m^2	D20, 5 cm ILH
Burning time	t	820	s	Fig. 10

$$h_C = L - \Delta/2$$
$$h_I = L + \Delta/2 \tag{7}$$

Δ is defined in Eq.(8)

$$\frac{\Delta}{L} = X\sqrt{1 - \frac{X^2}{16}} \tag{8}$$

Here, L is the flame height, and X is defined in Eq.(9).

$$X = \frac{1.27}{\sqrt{\frac{L}{D}}} \tag{9}$$

Here, L is the flame height and D is the pool diameter. The numerical factor 1.27 was given for heptane [38]. With these equations, the height of the cylindrical continuous flame (h_{cyl}) and the conical-shaped intermittent flame (h_{cone}) can be calculated by Eq. (10).

$$h_{cyl} = h_C$$
$$h_{cone} = h_I - h_C \tag{10}$$

Inserting values for the case above, one obtains $h_{\mathrm{cyl}} = 0.36$ m and $h_{\mathrm{cone}} = 0.42$ m.

Consider a plane at the container top with the flame above, see Fig. 18. Radiation from the container top will exclusively reach the flame (that is, the cylinder/cone flame structure). Therefore the view factor from the plane to the flame is equal to 1, as expressed in Eq. (11).

$$\varphi_{C\to F} = 1 \tag{11}$$

The repository law of view factors gives Eq. (12).

$$\varphi_{F\to C} = \frac{A}{A_F}\cdot\varphi_{C\to F} \tag{12}$$

Here, A is the area of the container cross-section, A_F is the inner area of the flame (calculated according to Fig. 18) and $\varphi_{F\to C}$ is the view factor from the flame to the container. Since $\varphi_{C\to F} = 1$, Eq. (12) can be rewritten as Eq. (13)

$$\varphi_{F\to C} = \frac{A}{A_F} \tag{13}$$

With area $A_F = 0.36$ m^2, and values from Table 2, $\varphi_{F\to C}$ is 0.087. Using Eq. (5), the radiation from the flame to the system ($\dot{Q}_F$) can be estimated as 550 ± 250 W.

The redistributed energy ($\dot{Q}_U$) can be estimated by Eq 14–16. Eq. (14) gives the energy flux required to evaporate fuel.

$$\dot{Q}_V = \dot{m}''\cdot A\cdot L_V \tag{14}$$

Here, L_v is the latent heat of evaporation. Using values from Table 2, the energy flux used to evaporate heptane ($\dot{Q}_V$) is 210 ± 14 W. Thus, only a small fraction of the heat-release rate (approximately 1%) from the combustion is used to evaporate fuel. This is in accordance with values reported by Koseki and Hayasaka [40].

Heat loss from the container $\dot{Q}_L$ consists of convective cooling at the outer container wall, see Eq. (15), radiation from the containers outer walls, see Eq. (16) and conductive heat loss through the container bottom (which is not included). Convective heat loss is estimated using Eq. (15).

$$\dot{Q}_{L,\,\mathrm{conv}} = h\cdot A_w\cdot\Delta T \tag{15}$$

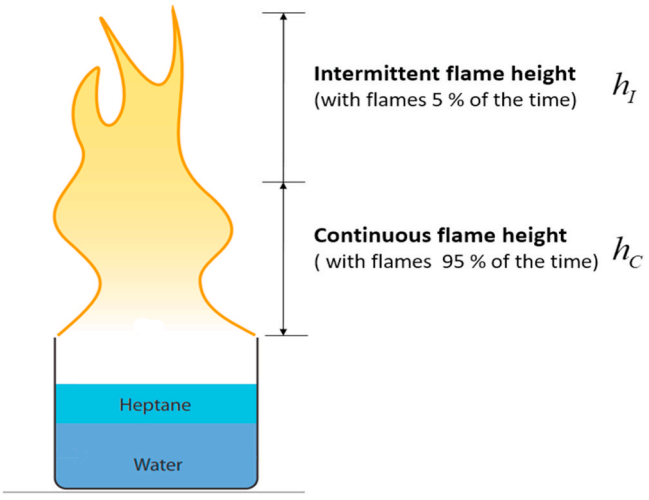

Fig. 17. Intermittent h_I and continuous flame height h_c with definitions.

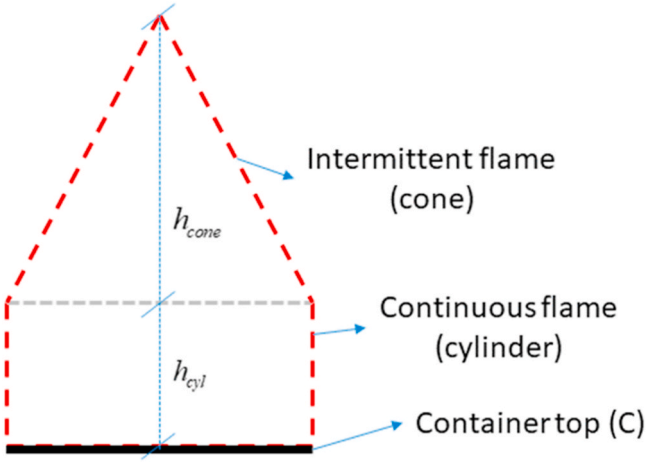

Fig. 18. Flame shape as proposed in Ref. [38], with the continuous part represented by a cylinder and the intermittent one by a cone. The dotted red lines outline the flame, the grey dotted line separates the continuous flame from the intermittent flame. The solid black line represents the container top. (For interpretation of the references to colour in this figure legend, the reader is referred to the Web version of this article.)

Here, h is the convective heat transfer coefficient (according to Holman [41] it is reasonable to assume $h = 10\ {}^{\mathrm{W}}/_{\mathrm{m}^2\cdot\mathrm{K}}$ in situations where one does not have a definite value for h), A_w is the area of the outer wall of the container, and ΔT is the temperature difference between the ambient atmosphere and the container wall. Using a wall temperature between 220 and 240 °C, from data in Fig. 10a and b, ΔT can be estimated as 210–230 °C. Using these values in Eq. (15) the convective heat loss from the container ($\dot{Q}_{L,\,\mathrm{conv}}$) can be estimated to be between 145 and 159 W.

Radiative heat losses from the outer container wall can be calculated using Eq. (16).

$$\dot{Q}_{L,\,\mathrm{rad}} = \varepsilon_s \sigma A_{w1} T^4 \tag{16}$$

Here, ε_s is the emissivity to the steel container, σ is the Stefan-Boltzmann constant, and A_{w1} is the area of the heated container wall, i.e., the part that neither is cooled by the heptane layer, nor by the water layer. The typical wall temperature is assumed to be 220–240 °C (see above). Thus, the absolute temperature (T) of the radiating wall is 493–513 K. Due to the low emissivity of polished stainless steel, the heat-loss rate from radiation $\dot{Q}_{L,\,\mathrm{rad}}$ is low, between 45 and 53 W, giving a total heat-loss rate ($\dot{Q}_L$) of between 190 and 212 W.

$$\dot{Q}_S = \frac{C_{p,i}\cdot m_i \cdot \Delta T}{t} = C_{p,i}\cdot \dot{m}''_i \cdot A \cdot \Delta T \tag{17}$$

The energy flow required to heat the steel container, the water and the heptane is $\dot{Q}_S$ [W] given in Eq. (17) where $C_{p,i}$ is the heat capacity, m_i is the mass, ΔT is the change in temperature and t is the duration of the experiment (burning time). The average increase in the water temperature through an experiment, was approximately 20 °C, this gives $\dot{Q}_{S,\,\mathrm{water}} = 128$ W. The container wall temperature typically increased 200–220 °C and 20 °C, for container above and below the water level, respectively. Using values from Table 2 the flux associated with energy stored in the container is $\dot{Q}_{S,\,\mathrm{container}} = 42$ W. The heptane was heated from ambient temperature to its boiling point at 98 °C, so $\dot{Q}_{S,\,\mathrm{hept}}$ is then 14 W. The total energy flow associated with energy storage ($\dot{Q}_S$) is then 184 W.

$$\dot{Q}_U = \dot{Q}_V + \dot{Q}_L + \dot{Q}_S \tag{18}$$

When summing the different energy flows, $\dot{Q}_U$ becomes between 600 ± 25 W, which is consistent with the estimated $\dot{Q}_F$ of 550 ± 250 W.

As described by Akita and Yomoto [20], there are vortices transporting energy from the flame to the fuel surface by convection. This convective energy flow can be calculated using Eq. (15) with $h = 5.7\ {}^{\mathrm{W}}/_{(\mathrm{m}^2\mathrm{K})}$ as proposed by Hottel [30], A as the fuel surface area, and an assumed temperature difference $\Delta T = 850$ °C[38] between the flame and the fuel at its boiling point (98 °C). Eq. (15) gives a convective energy flow at 150 W. With the convective contribution the energy received by the container $\dot{Q}_F$ increases to 700 ± 250 W. Even with the convective contribution the conservation of energy is preserved, $\dot{Q}_U$ is still consistent with $\dot{Q}_F$.

Even though $\dot{Q}_F$ and $\dot{Q}_U$ are sensitive to variations in the used values, this simplified heat balance gives useful insight in how the energy from the fire is redistributed in the system. Considering the overall energy balance, the results indicates that 35% of the energy flux is used to evaporate the fuel ($\dot{Q}_V$), 35% is emitted ($\dot{Q}_L$) from the system and 30% is stored ($\dot{Q}_S$) through increased temperatures within the system. Thus, the estimates above, with all inherent simplifications, lead to a consistent description of the heat exchanges between the system (steel container, heptane layer and water layer) and its surroundings. This description may serve as a basis for a more sophisticated heat-flow model later.

The lip height affects the mass flux of a pool fire, which in its turn affects the temperatures in the container. A higher lip height gives a lower mass flux (see, e.g., Fig. 14) and thereby a lower heat flux. An increased lip height will lead to heating of a larger container wall area, which leads to higher energy losses through convection and radiation from the container wall to the surroundings. The energy used to evaporate the fuel will also decrease, since more energy is used for heating the container wall and emitted from the container. Thus, the distribution of the incoming energy may be different from the case discussed above for other values of lip height and container diameter.

5. Conclusion

In this work on batch pool fires (without refilling of fuel), the effect of increasing lip heights has been investigated. The fires lasted 12–14 min for partly filled containers (with heptane on top of a water layer) and 1–2 h for containers filled with heptane only. Three main findings are:

First, the mass loss rate ($\dot{m}$) decreases with increasing lip height, which is in accordance with earlier studies. The reduction in $\dot{m}$ is up to 36% compared with experiments with no initial lip height. The significant reduction in mass-loss rate due to lip height should be accounted for in fire calculations and fire simulations.

Second, the lip-height effect can surpass the pool-size effect (diam-

eter) with respect to mass-loss rate/mass flux. This can be seen clearly by comparing a small container with low lip height, with a larger container with high lip height. A D20 container with 2 cm initial lip height versus a D30 container with 8 cm initial lip height gives mass fluxes of $\dot{m}'' = 27\ {}^{g}/_{m^2 s}$ and $\dot{m}'' = 24\ {}^{g}/_{m^2 s}$ respectively. The latter had lower $\dot{m}''$ than the former, despite a larger diameter. Therefore, for the investigated containers the lip height is as important for the mass-loss rate as the pool dimeter.

Third, the energy flux received by the system from the flame is, for one case considered in detail, distributed as follow: Approximately 1/3 (35%) was emitted to the surroundings and 1/3 (30%) heated the container, fuel, and water layer. The last 1/3 (35%) was used to evaporate fuel. Our results illustrate the complexity of pool fires and emphasize the importance of including lip height both in mass-loss and heat-production calculations.

Funding sources

This research did not receive any specific grant from funding agencies in the public, commercial, or not-for-profit sectors.

Author Statement

All authors have contributed to developing the experimental setup, research question, and methods used for analysis of data. The first author (E.A.K.) has carried out experiments and analyses. All authors have contributed to the manuscript and its revisions.

Declaration of competing interest

The authors declare that they have no known competing financial interests or personal relationships that could have appeared to influence the work reported in this paper.

References

[1] B. Karlsen, J.G. Quintiere, Enclosure Fire Dynamics, CRC Press LLC, 2000.
[2] NIST, Fire Dynamic Simulator, Validation Guide, 2017, p. 470.
[3] C. L. Beyler, " Fire hazard calculations for large, open hydrocarbon fires," in *SFPE Handbook Of Fire Protection Engineering*, New York, NY, Springer New York, pp. 2591-2663.
[4] H. Malvos, P.k. Raj, Thermal Emission and Other Characteristics of Large Liquefied Natural Gas Fires, " *Wiley InterScience*, 26 December 2006.
[5] V. Babrauskas, R.D. Peacock, Heat release rate: the single most important variable in fire hazard, Fire Saf. J. 18 (1992) 255–272.
[6] V.I. Blinov, G.N. Khudiakov, Certain Laws Governing Diffusive Burning of Liquids, 1957.
[7] Blinov, Khudiakov, Diffusion Buring of Liquids, US army Translation, 1961.
[8] D. Burgess, M.G. Zabetakis, Fire and Explosion Hazards Associated with Liquefied Natural Gas, U. S. Dept. of the Interior, Bureau of Mines, Washington, 1962.
[9] E.S. Artemenko, B. V. I., Burning of liquids in vessels with change of levels, Fiz. Goreniya i Vzryva 4 (1) (1968) 69–75.
[10] H.W. Emmons, Some observetions on pool burning, International Symposium on the Use of Models in Fire Research (July 1961) 50–67.
[11] C. Liu, L. Ding, M. Jangi, J. Ji, L. Yu, H. Wan, Experimental study of the effect of ullage height on flame characteristics of pool fires, Combust. Flame (2 April 2020) 245–255.
[12] C. Tao, X. Wang, P. Ma, P. Zhu, An experimental investigation on mass burning rate of small hydrocarbon pool fires with different lip heights, J. Chin. Inst. Eng. (4 Februar 2019) 169–174.
[13] B.Z. Dlugogorski, M. Wilson, Effect of lip height on properties of small scale pool fires, Fire Saf. Sci. (1995) 129–140.
[14] E.A. Kolstad, V. Frette, B.C. Hagen, Lip height effect in quadrangular steel containers, in: InterFlam, 2019.
[15] L. Orloff, Simplified radiation modeling of pool fires, Eighteenth Symposium (international) on Combustion (1981) 549–561.
[16] L. Orloff, J. de Ris, Froude modeling of pool fires, in: Nineteenth Symposium (International) on Combustion, The Combustion Institute, 1982, pp. 885–895.
[17] L. Hu, J. Hu, J.L. de Ris, Flame necking-in and instability characterization in small and medium pool fires with different lip hights, Combust. Flame (2015) 1095–1103.
[18] A. Bouhafid, J.P. Vantelon, P. Joulain, A.C. Fernandez-Pello, On the flame structure at the base of pool fires, in: 22nd Symposium (International) on Combustion, 1988, pp. 1291–1298.
[19] H. Hayasaka, Unsteady burning rates of small pool fires, in: Fire Safety Science-Proceedings Of the Fifth International Symposium, Melbourn, Australia, 1997.
[20] K. Akita, T. Yumoto, Heat transfer in small pools and rates of burning of liquid methanol, in: Tenth Symposium (International) on Combustion, 1965, pp. 943–948.
[21] A. Nakakuki, Heat mechanisms in liquid pool fires, Fire Saf. J. (30 June 1994) 339–363.
[22] A. Nakakuki, Heat transfer in small scale pool fires, Combust. Flame (1994) 311–324.
[23] A. Nakakuki, Heat transfer in pool fires at a certaun small lip height, Combust. Flame (2002) 259–272.
[24] A. Hamins, S.J. Ficher, T. Kashiwagi, M. E. K. a. J. P. Gore, Heat feedback to fuel surface in pool fires, Combust. Sci. Technol. (26 February 1993) 37–62.
[25] L. Hu, S. Liu, L. Wu, Flame radiation feedback to fuel surface in medium ethanol and heptane pool fires with cross air flow, Combust. Flame (11 October 2013) 295–306.
[26] A. Shinotake, S. Koda, K. Akita, An experimental study of radiative properties of pool fires of an intermediate scale, Combust. Sci. Technol. (July 1984) 85–97.
[27] P. Joulain, The behcaviour of pool fires: the art and new insights, in: Twenty-Seventh Symposium (International) on Combustion, 1998, pp. 2691–2706.
[28] L. Hu, A Review of physics and correlations of pool fire behaviour in wind and furture challenges, Fire Saf. J. (5 May 2017) 41–55.
[29] B.D. Dich, J.L. de Rise, T.K. Blanchat, M. Chaos, R.G. Bill Jr., S.B. Borofeev, Pool fires - an empirical correlation, Combust. Flame (2013) 2964–2974.
[30] H.C. Hottel, Certain laws governing diffusive burning of liquids, Fire Research Abstracts and Reviews (September 1958) 41–44.
[31] V. Babrauskas, Estimating large pool fire burning rates, in: Fire Technology vol. 19, 1983, pp. 251–261.
[32] C. Kuang, L. Hu, X. Zhang, Y. Lin, L.W. Kostiuk, An experimental study on the burning rates of n-heptane pool fires with various lip heights in cross flow, Combust. Flame (20 Desember 2019) 93–103.
[33] D. Drysdale, An Introduction to Fire Dynamics, third ed., Wiley, 2011.
[34] National Institute of Standards and Technology, NIST Chemistry WebBook, SRD 69, NIST, 2018 [Online]. Available, https://webbook.nist.gov/cgi/cbook.cgi?ID=C142825&Mask=4. (Accessed 30 May 2021).
[35] National Institute of Standards and Technology, NIST Chemistry WebBook, SRD 69, NIST, 2018 [Online]. Available, https://webbook.nist.gov/cgi/cbook.cgi?ID=C142825&Mask=2. (Accessed 31 May 2021).
[36] J.R. Howell, R. Siegel, M.P. MEngüç, Thermal Radiation Heat Transfer, fifth ed., CRC Press, Tayler and Francis Group, 2011.
[37] Iron Boar Labs Ltd, makeitfrom.com, Iron Boar Labs Ltd, 20 May 2020 [Online]. Available, https://www.makeitfrom.com/material-properties/AISI-304-S30400-Stainless-Steel. (Accessed 3 June 2020).
[38] G. Shen, K. Zhou, F. Wu, J. Jiang, A model considering the flame volume for prediction of thermal radiationfrom pool fire, Fire Technol. 55 (January 2019) 129–148.
[39] G. Heskestad, Peak gas velocities and flame heights of buoyancy-controlled turbulent diffusion flames, Proc. Combust. Inst. (1981) 951–960.
[40] H. Koseki, H. Hayasaka, Estimation of thermal balance in heptane pool fire, J. Fire Sci. (1 July 1989) 237–250.
[41] J.P. Holman, Heat Transfer, 10th ed., McGraw-Hill, New York, 2010.